Authors for correspondence:
Hamza Ahmad Isiyaka
e-mail: hamza_18001996@utp.edu.my
Nonni Soraya Sambudi
e-mail: soraya.sambudi@utp.edu.my

Removal of 4-chloro-2-methylphenoxyacetic acid from water by MIL-101(Cr) metal-organic framework: kinetics, isotherms and statistical models

Hamza Ahmad Isiyaka[1], Khairulazhar Jumbri[1], Nonni Soraya Sambudi[2], Zakariyya Uba Zango[1], Bahruddin Saad[1] and Adamu Mustapha[3]

[1]Fundamental and Applied Sciences Department, and [2]Chemical Engineering Department, Universiti Teknologi PETRONAS, Bandar Seri Iskandar 32610, Perak Darul Ridzuan, Malaysia
[3]Department of Geography, Faculty of Earth and Environmental Science, Kano University of Science and Technology, Wudil, 3244 Kano Postal, Nigeria

HAI, 0000-0002-6331-8134; KJ, 0000-0003-3345-6453

Effective removal of 4-chloro-2-methylphenoxyacetic acid (MCPA), an emerging agrochemical contaminant in water with carcinogenic and mutagenic health effects has been reported using hydrothermally synthesized MIL-101(Cr) metal-organic framework (MOF). The properties of the MOF were ascertained using powdered X-ray diffraction (XRD), Fourier transform infrared (FTIR) spectroscopy, thermal gravimetric analysis (TGA), field emission scanning electron microscopy (FESEM) and surface area and porosimetry (SAP). The BET surface area and pore volume of the MOF were 1439 $m^2\,g^{-1}$ and 0.77 $cm^3\,g^{-1}$, respectively. Artificial neural network (ANN) model was significantly employed for the accurate prediction of the experimental adsorption capacity (q_e) values with minimal error. A rapid removal of the pollutant (99%) was recorded within short time (approx. 25 min), and the reusability of the MOF (20 mg) was achieved up to six cycles with over 90% removal efficiency. The kinetics, isotherm and thermodynamics of the process were described by the pseudo-second-order, Freundlich and endothermic adsorption, respectively. The adsorption process is spontaneous based on the negative Gibbs free energy values. The significant correlation between the experimental findings and simulation results suggests the great potential of MIL-101(Cr) for the remediation of MCPA from water matrices.

1. Introduction

Over the last decades, there has been scientific detection and identification of new emerging pollutants that contaminate surface and groundwater resources [1]. These compounds and their metabolites are found to endanger human health as well as destroy aquatic animals [2]. Evidence from previous studies have shown that agrochemicals such as 4-chloro-2-methylphenoxyacetic acid (MCPA) have immensely contributed to water pollution through agricultural runoff, direct spray and leaching [3,4]. MCPA is among the most extensively used herbicides that have been applied to selectively control weeds in farmlands, roads and gardens [5,6]. It has a high water solubility of 825 mg l^{-1} with a field half-life of 31 days [7]. When excessively applied, their residues may remain in the soil, thereby making it easily available to runoff, and to be leached down to contaminate surface and groundwater [8]. Thus, it is easily transported from a point source to non-point sources over long distance [9]. Some of the physico-chemical properties of the MCPA are highlighted in table 1.

MCPA can easily bioaccumulate and be biomagnified in the tissues of plants and aquatic animals and cause serious health risk to humans [10]. The uncontrolled discharge of this pollutant has significantly contributed to the scarcity of clean water for consumption and other domestic use, particularly in developing countries with high population, agricultural dependent and poor living standard [11]. According to the World Health Organization (WHO), as of 2015, an estimate of 663 million people do not have access to clean water, and by 2050, one in every four persons will consume contaminated water in developing nations [12]. The United States Environmental Protection Agency (USEPA) have listed MCPA as priority pollutant with possible carcinogenic and mutagenic effects [13]. The maximum standard limit for MCPA in drinking water is set by the WHO and USEPA as 0.1 µg l^{-1} [14]. These shortfalls motivate scientists and researchers to search for practical methods for wastewater treatment.
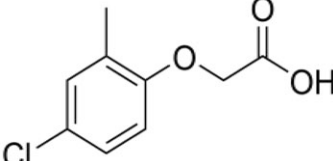
Over the years, various remediation techniques such as coagulation, flocculation, membrane filtration, precipitation, ion exchange, chemical oxidation, biodegradation and adsorption have been applied to remove pollutants from water [15]. Of these methods, adsorption has been singled out to be the most practical and promising technique due to its low cost, simple operations, high selectivity, environmentally benign, convenient recycling and availability of various adsorbents materials [16]. Some adsorbents such as activated [17,18], biochar [19], clay minerals [8] and goethite [20] have been previously used for MCPA adsorption. However, the ideal adsorbent is expected to possess a relatively high surface area, large pore volume, good water and thermal stability under harsh condition [21]. Thus, the quest for finding the best adsorbent materials seems limitless.

Metal-organic frameworks (MOFs) have been substantial applied in different fields due to their peculiar properties for versatile application. They have been considered as one of the highly porous and advanced materials recently discovered [22,23]. MOFs have quickly attracted the attention of researchers for various applications such as CO_2 capture, gas storage, sensing, catalysis, biomedical imaging and wastewater remediation [24,25]. They are highly porous, crystalline materials with ultra-high surface area, consisting of metal clusters and multifunctional organic linkers [25].

Among the several MOFs reported, the Materials Institute Lavoisier (MILs) class are exceptionally promising material that have been applied for the remediation of contaminants such as pharmaceuticals, dyes and heavy metals [26,27] in wastewaters. The MIL-101(Cr) is formed from a combination of chromium (III) oxide octahedral trimmers and dicarboxylate linker, resulting in a high class of hybrid supertetrahedron azeotypic mesoporous MOF [28]. The chemical stability of this MOF improves with increasing inertness of the central metal ions and the thermal stability can be explained by the strength of the metal oxygen bond. This is due to the remarkable inertness of Cr(III) that allows the formation of strong Cr-O bond [29]. This MOF is very rigid with large surface area and pore size. MIL-101(Cr) was recently applied by Mirsoleimani-Azizi *et al.* [30] for the removal of pesticide (diazinon) in an aqueous medium. High removal efficiency (92.5%) was achieved. The high adsorption capacity of dyes (377–392 mg g^{-1}) was recorded by MIL-101(Cr) with a fast removal efficiency of 99.9% within 30 min [31]. Another study conducted by Gao *et al.* [32] shows rapid removal of pharmaceuticals by MIL-101(Cr) within 60 min. These applications outperformed most of the previous materials applied for the remediation of contaminants in water.

Adsorption process involves nonlinear relationships between several factors that are difficult to model using conventional methods. In previous studies, only one parameter is varied at a time without modelling the simultaneous interaction between the critical adsorption parameters (contact time, initial concentration, dosage, pH and temperature). Limited works have been carried out to

Table 1. Some properties of the studied herbicide.

common name	chemical name	molecular formula	structure	solubility (mg l^{-1})	pKa	log P
MCPA	4-chloro-2-methylphenoxyacetic acid	$C_9H_9ClO_3$		8.25	3.13	2.8

model and predict the interactive adoption behaviour of MCPA onto MIL-101(Cr). Thus, this study introduces the artificial neural network (ANN) model to evaluate and model the adsorption process and interaction between the adsorption parameters. The ANN is used for the prediction of the experimental findings through learning the pattern of the process. ANN can be trained to develop a non-parametric relationship between multiple input parameters that control the adsorption process [33]. It is a model that mimics the human brain as such does not require prior knowledge of the process controlling the adsorption system. Thus, the aim of this study is to evaluate the removal efficiency of MIL-101(Cr) metal-organic framework for the adsorption of MCPA in an aqueous medium. Batch adsorption experiment has been used to study the effect of the parameters, kinetics and isotherm of the process. ANN was used to model and predict the nonlinear relationship of the adsorption process under the said experimental conditions.

2. Material and methods

2.1. Materials

Chromium nitrate nonahydrate ($Cr(NO_3)_3 \cdot 9H_2O$, 99%), 1,4-benzene dicarboxylic acid (H_2BDC, 99%), N,N-dimethyl formamide (DMF, 99%), methanol (99.5%), ethanol (99.9%) hydrochloric acid and sodium hydroxide were of analytical grade and supplied by Avantis Laboratory (Ipoh Perak, Malaysia) and were used without further purification. MCPA with 98% purity was purchased from Sigma-Aldrich (St Louis, MO, USA).

2.2. Synthesis of MIL-101(Cr) adsorbent

MIL-101(Cr) was hydrothermally synthesized according to the previous procedure [34] using $Cr(NO_3)_3 \cdot 9H_2O$ (8 g), H_2BDC (3.32 g) and deionized water (100 ml). The mixture was stirred for 30 min using a magnetic stirrer. HF (10 mmol) was gradually added to the mixture and stirred for 15 min. The mixture was placed in a stainless-steel Teflon-lined autoclave, sealed and inserted into a preheated electric oven at 483 K for 8 h. Next, the autoclave was allowed to cool to room temperature and the product was filtered and recovered. The as-synthesized product was further purified using deionized water, DMF and ethanol to remove possible impurities in the pores. The product yield reached as high as 89%. The purified product was finally dried overnight, cooled to room temperature and stored in a desiccator.

2.3. Characterization of MIL-101(Cr) adsorbent

The crystallinity and structural properties of the MIL-101(Cr) were recorded on a Bruker D8 Advance X-ray diffraction (XRD). The thermal stability of the adsorbent was assessed by thermogravimetric analysis (TGA) under N_2 atmosphere using Shimadzu TGA-50 Analyser which was heated from 30 to 800°C at a heating rate of 10°C min^{-1}. The functional group of the material was determined using Perkin Elmer FTIR Spectrometer which was scanned from 400 to 4000 cm^{-1}. Field emission scanning electron microscopy (FESEM) was used to determine the morphology using Zeiss Supra 55 VP

instrument, while the BET surface area and pore size were analysed using N_2 adsorption–desorption with Micromeritics ASAP 2020.

2.4. Batch adsorption studies

Adsorption experiments were carried out by preparing a stock solution of MCPA (1000 mg l^{-1}) by dissolving 100 mg of the analyte in a 1000 ml volumetric flask containing water and was kept in a refrigerator (0°C) prior to use. From the stock, solutions containing different initial concentrations (5–50 mg l^{-1}) were studied by dispersing 20 mg of MIL-101(Cr) adsorbent in 100 ml conical flask. The total volume used for each experiment was 50 ml. The flask was then inserted into a thermostatic incubator shaker (incubator ES 20/60, Biosan) and agitated at 150 r.p.m. for 5–60 min. The sample solution (2 ml) was collected and filtered with a nylon syringe membrane (0.45 µm) at every 5 min interval. The absorbance of the MCPA solutions was measured with a UV-Vis spectrophotometer (Shimadzu, Lamda 25). The effects of pH and temperature were studied by adjusting the initial pH from 2 to 12 using either 0.1 M HCl or 0.1 M NaOH, while the temperature was varied from 25 to 50°C. The effect of dosage was also studied by varying the dose from 5 to 50 mg. All the adsorption data were recorded in triplicate from which the average values were calculated.

The quantity of MCPA adsorbed at equilibrium (q_e), percentage removal (%R) and quantity adsorbed at a time interval (q_t) were calculated using the following equations:

$$q_e = \frac{(C_o - C_e)V}{w} \tag{2.1}$$

$$\%R = \frac{(C_o - C_t)}{C_o} \times 100 \tag{2.2}$$

and
$$q_t = \frac{(C_o - C_t)V}{w}, \tag{2.3}$$

where C_o, C_t and C_e are the initial, time and equilibrium concentration of MCPA (mg g–1), V is the volume of the solution (l) and w is the weight of the adsorbent (g).

2.5. Artificial neural network model

ANN mimics the behaviour of the human brain in processing information and can learn, predict and correlate the pattern of experimental data when subjected to training [35,36]. The technique provides a platform that can determine the impact of some optimized adsorption parameters in the behaviour of a target output. In this study, the multilayer-perceptron feed-forward-neural network (MLP-FF-ANN) with a back-propagation algorithm and log-sigmoid activation function [37] was used to predict the adsorption capacity of MCPA onto MIL-101(Cr) in correlation with the experimental result. The network structure of the MLP-FF-ANN consists of multiple neurons that are organized in layers. The number of hidden neurons was determined on the basis of trial and error, which forms the training process [38]. The dataset was divided into training (60%), testing (20%) and validation (20%). The network was trained by adjusting the weight to learn the data pattern, and the testing subset was used to evaluate the generalization ability of the network, while the validation datasets were used to estimate the network efficiency. Using these models, criteria such as coefficient of determination (R^2), adjusted R^2 (R^2adj), root mean square error (RMSE) and Akaike information criteria (AIC) are considered as the best fit to judge the performance of our adsorption process by regression analysis. The following equations were used:

$$R^2 = 1 - \frac{\sum (x_i - y_i)^2}{\sum y_i^2 - (\sum y_i^2 / n)}, \tag{2.4}$$

$$R_{adj}^2 = 1 - (1 - R^2)\left(\frac{n-1}{n-p}\right), \tag{2.5}$$

$$\text{RMSE} = \sqrt{\frac{1}{n}\sum_{i=1}^{n}(x_i - y_i)^2} \tag{2.6}$$

and
$$\text{AIC} = n\ln\left(\frac{\text{SSE}}{n}\right) + 2n_p + \frac{2n_p(n_p + 1)}{n(n_p + 1)}, \tag{2.7}$$

where x_i represents the observed data that was determined experimentally, y_i is the predicted data, n is the number of observation and p denotes the number of parameters.

2.6. Adsorption isotherms

Adsorption isotherms provide information on the type of interaction mechanism that exists between MIL-101(Cr) and the studied herbicide. It describes the amount of pollutants adsorbed per unit weight of an adsorbent and the residual pollutant concentration in solution at equilibrium. The Langmuir, Freundlich and Temkin isotherms were used to describe the adsorption of MCPA onto MIL-101(Cr). The models are described by the following equations [39].

Langmuir model

$$\frac{C_e}{q_e} = \frac{1}{K_L q_m} + \frac{C_e}{q_m} \tag{2.8}$$

and

$$R_L = \frac{1}{1 + C_o K_L}, \tag{2.9}$$

where C_e is the concentration at equilibrium (mg g^{-1}), q_e is the quantity of MCPA adsorbed at equilibrium (mg g^{-1}), q_m and K_L are the constants representing adsorption capacity and adsorption energy, respectively. R_L depicts the favourability of the adsorption process ($R_L > 1$, unfavourable; $0 < R_L < 1$, favourable; $R_L = 1$, linear).

Freundlich model

$$\log(q_e) = \log K_F + \frac{1}{n} \log C_e, \tag{2.10}$$

where K_F is the Freundlich constant of adsorption capacity, n is the adsorption intensity and C_e is the equilibrium concentration of MCPA (mg g^{-1}).

Temkin model

$$q_e = B \ln A_T + B \ln C_e, \tag{2.11}$$

where B is the heat of adsorption (J mol^{-1}) and A_T is the Temkin equilibrium binding constant corresponding with the maximum binding energy (l g^{-1}).

2.7. Adsorption kinetics model

The adsorption rate, reaction mechanism and equilibrium time are fundamental in determining the effectiveness and efficiency of the adsorbent material as well as the mass transfer which explains the rate-limiting steps [40]. The pseudo-first-order, pseudo-second-order and intraparticle diffusion model were used to ascertain the best fitting for the experimental data.

Lagergren pseudo-first-order model

$$q_t = q_e(1 - e^{-k_1 t}). \tag{2.12}$$

Pseudo-second-order model

$$q_t = \frac{K_2 q_e^2 t}{1 + K_2 q_e t}. \tag{2.13}$$

Intraparticle diffusion model

$$q_t = K_P t^{0.5} + C, \tag{2.14}$$

where q_t and q_e are the amounts of MCPA adsorbed at certain equilibrium and time t (mg g^{-1}), K_1 (min^{-1}) is the pseudo-first-order rate constant, K_2 (g mg^{-1} min^{-1}) is the equilibrium rate constant of the pseudo-second-order, and the intraparticle diffusion rate constant is represented as K_p (mg g^{-1} min^{-1}).

2.8. Thermodynamics studies

The Gibbs free energy change ($\Delta G°$), enthalpy change ($\Delta H°$) and entropy change ($\Delta S°$) were used to determine the feasibility of the adsorption process based on the temperature changes. This helps to

describe whether the adsorption process is spontaneous, exothermic or endothermic. The equations are

$$G° = -RT \ \ln K_C \tag{2.15}$$

and

$$G° = H° - TS°, \tag{2.16}$$

where $\Delta G°$ is the free energy (J K mol^{-1}), T (K) and R (J K mol^{-1}) are the temperature and universal gas constant for the adsorption, respectively and K_C is the equilibrium constant.

2.9. Reusability studies

The reusability of MIL-101(Cr) was studied to assess its potential for regeneration. After the adsorption experiments, the supernatant was decanted, filtered and washed with acetone and distilled water several times. The MOF was vacuum dried for 4 h at 80°C and reused as an adsorbent for the removal of MCPA in water. The process was repeated for six consecutive cycles and the removal of the herbicide was calculated for each cycle.

3. Results and discussion

3.1. Characterization of MIL-101(Cr)

The diffraction pattern of the obtained MIL-101(Cr) (figure 1a) indicates peaks that are in agreement with those reported in the previous studies [31,41], confirming a well-formed crystalline structure of the MIL-101(Cr). The FTIR spectra of the MOF is presented in figure 1b. The peak at 567 cm^{-1} is attributed to the Cr-O bond which depicts the formation of a well-structured material, and the bands at 746 and 1287 cm^{-1} are assigned to the C-H bond [42]. The peak at 1384 cm^{-1} depicts the symmetric vibration indicating the presence of dicarboxylate group in the MOF [43]. The peak at 1581 cm^{-1} denotes C=C stretching vibration [44], and the strong-broad band at approximately 3433 cm^{-1} shows the presence of O-H group in the material [32]. TGA reveals the thermal stability of the MIL-101(Cr) adsorbent. Three stages of weight loss were observed in figure 1c. The first weight loss is found in the temperature range of 5–200°C. The second weight loss is at approximately 200–308°C, attributed to desorption of adsorbed guest molecules from the pores. The third weight loss (308–600°C) denotes complete decomposition of terephthalic acid in the framework. The MOF was completely decomposed at 800°C, in agreement with an earlier study [41]. The FESEM image of the MIL-101(Cr) (figure 1d) corresponds to an octahedral crystalline structure similar to the previously reported study [42]. The elemental composition at the surface of the MOF as shown in the EDX (figure 1d) contains chromium (38.4%), oxygen (38%) and carbon (23.6%). The surface area and pore size of the MIL-101(Cr) was determined by Brunauer–Emmett–Teller (BET) under N$_2$ adsorption–desorption. The BET surface area of the MOF is approximately 1439 m^2 g^{-1} as detailed in table 2.

3.2. Artificial neural network prediction model

To develop the best ANN model for accurate prediction requires a careful selection and design of the network architecture, input combinations and model uncertainties [45]. A total of 264 experimental datasets obtained through the Design Expert 11 software were used to train, test and validate the ANN model. Several hidden neurons (table 3) were trained based on a trial and error approach to arrive at the best combination for the prediction of MCPA adsorption capacity, q_e (mg g^{-1}). The best ANN architecture comprising 5–8–1 topology (figure 2) was obtained during the training process. The input layer of the selected ANN topology comprises five parameters (contact time, initial concentration, adsorbent dosage, pH and temperature), the hidden layer has eight neurons and the output layer makes up one predicted response (adsorption capacity for MCPA, q_e (mg g^{-1})). The 5–8–1 topology gave the most significant predicted values indicating a better correlation between the experimental and observed datasets with R^2 0.998, 0.999, 0.981 and RMSE 0.088, 0.024, 0.066 for training, testing and validation, respectively (table 3). The scatter plots for the training, testing and validation subsets that show the correlation between the experimental and predicted values are presented in figure 3. The ANN model was also applied to predict the batch adsorption experimental q_e values for each range of experimental conditions in table 4. The result shows a significant
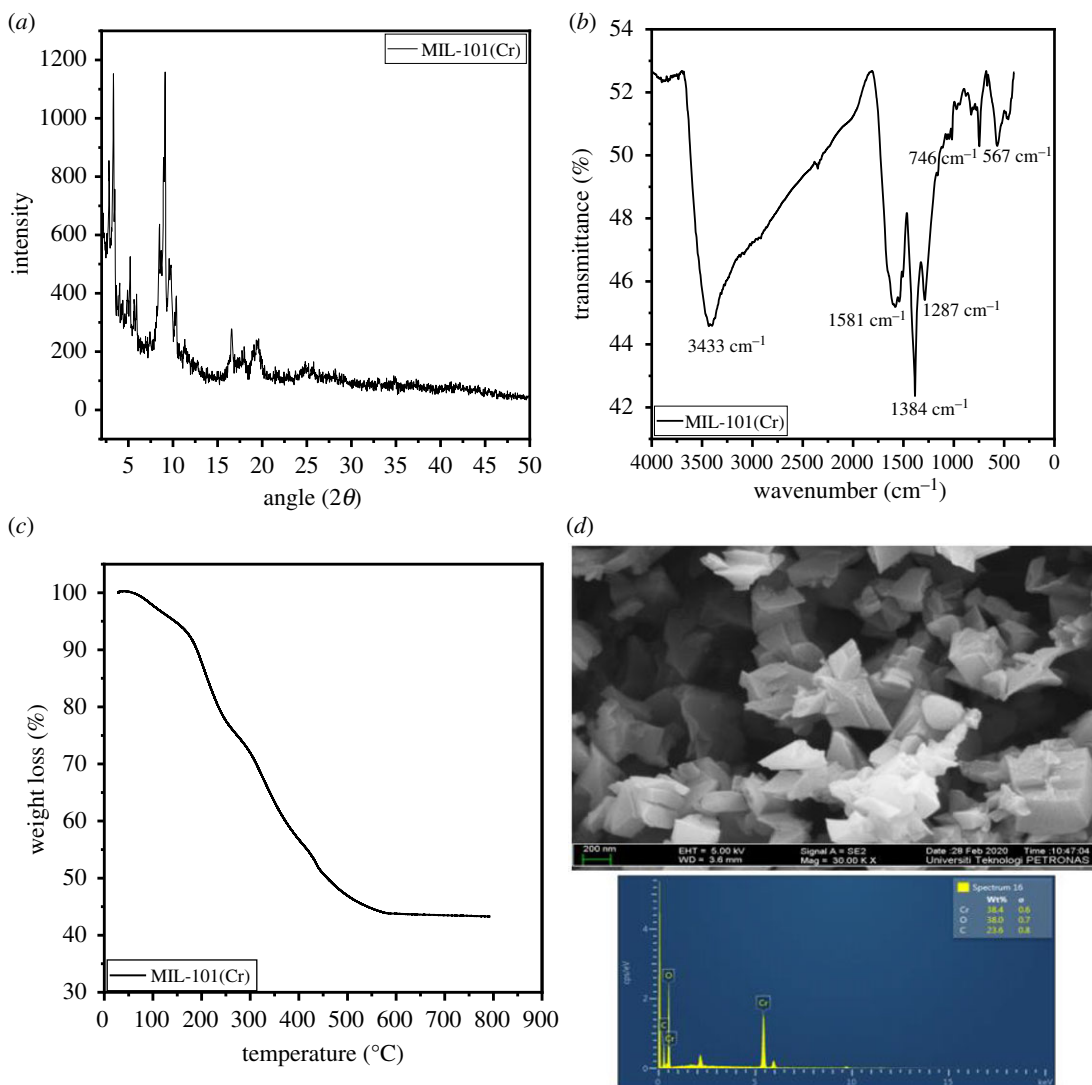
Figure 1. (*a*) XRD pattern, (*b*) FTIR spectrum, (*c*) TGA thermogram and (*d*) FESEM-EDX spectrum of MIL-101(Cr).

Table 2. BET surface area of MIL-101(Cr) MOF.

properties	MIL-101 (Cr)
BET surface area (m^2 g^{-1})	1439
Langmuir surface area (m^2 g^{-1})	2124
micropore surface area (m^2 g^{-1})	182
pore size (nm)	0.773

correlation between the experimental q_e and the predicted q_e values with minimal errors recorded. The predicted q_e is in agreement with the pseudo-second-order kinetics (q_e, experimental and q_e, calculated), indicating the potential of ANN as a technique for predicting wastewater remediation. This can be attributed to the ability of the ANN to learn the complexity of a dataset when subjected to training and can also model the nonlinear relationship between the actual and predicted variables.

3.3. Optimization studies of adsorption parameters

3.3.1. Effect of pH in the adsorption process

The initial pH condition of MCPA solution is a key parameter that determines the adsorption process and capacity. In this study, the effect of pH was investigated by varying the pH at the range of 2–12, herbicide
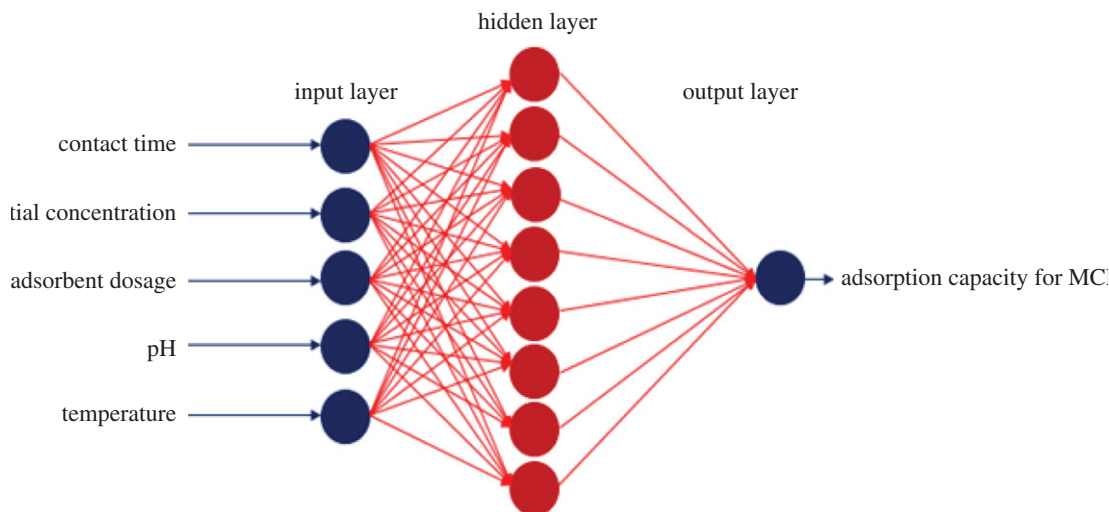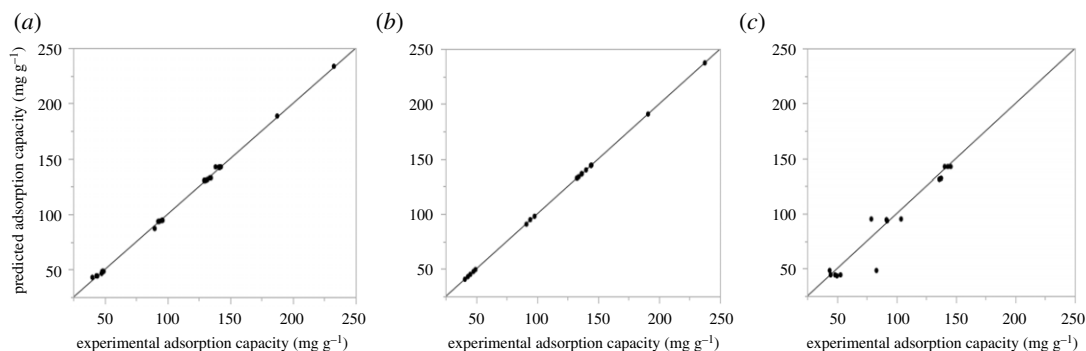
Figure 2. Artificial neural network topology.

Figure 3. Experimental and Predicted ANN scatter plots (*a*) training, (*b*) testing and (*c*) validation.

Table 3. Optimum ANN architecture for the prediction of MCPA adsorption capacity.

no.	neurons	training			testing			validation		
		R^2	R^2adj	RMSE	R^2	R^2adj	RMSE	R^2	R^2adj	RMSE
1	[3]	0.985	0.920	1.723	0.989	0.983	1.541	0.977	0.962	1.750
2	[4]	0.996	0.953	0.686	0.997	0.994	0.612	0.978	0.971	0.608
3	[5]	0.986	0.981	1.511	0.988	0.981	1.420	0.986	0.981	1.407
4	[6]	0.998	0.985	1.095	0.999	0.997	1.201	0.977	0.970	1.540
5	[7]	0.997	0.991	2.188	0.998	0.995	2.321	0.967	0.918	3.053
6	[8]	0.998	0.996	0.088	0.999	0.997	0.024	0.981	0.979	0.066
7	[9]	0.998	0.994	1.620	0.990	0.988	1.511	0.965	0.964	1.657
8	[10]	0.996	0.987	2.797	0.989	0.981	2.833	0.982	0.981	4.729
9	[5 5]	0.988	0.913	1.668	0.932	0.931	0.321	0.941	0.930	0.944
10	[5 7]	0.934	0.922	0.392	0.912	0.908	1.443	0.910	0.906	1.321
11	[7 6]	0.911	0.902	1.866	0.905	0.910	1.832	0.909	0.899	1.612

concentration (20 mg l^{-1}), dosage (20 mg) and temperature (40°C) as displayed in figure 4. At pH value higher than the pKa of MCPA (3.13), the herbicides solution will be predominantly in the anionic form (negatively charged) due to deprotonation. On the other hand, the surface of MIL-101(Cr) is positively charged at low pH (4–6) and negatively charged when the pH is high (>6). Hence, adsorption at high pH is very low due to the relatively weak interaction between the adsorbent and the herbicide molecule. Thus, a fast and higher removal of 98.62% is observed at

Table 4. Comparison between the experimental and predicted MCPA adsorption capacity, q_e (mg g^{-1}).

runs	contact time (min)	initial concentration (mg l^{-1})	adsorbent dosage (mg)	pH	temperature (°C)	experimental, q_e (mg g^{-1})	predicted, q_e (mg g^{-1})	error
1	15	20	20	4	30	93.620	91.878	1.742
2	5	10	30	2	35	44.388	44.208	0.180
3	15	20	40	4	30	94.585	94.516	0.429
4	15	20	20	8	30	92.173	92.610	0.437
5	25	40	20	4	30	188.577	188.445	0.132
6	25	10	10	2	35	48.379	49.236	0.857
7	15	20	20	4	45	94.585	95.661	1.076
8	5	30	10	2	35	130.441	131.085	0.644
9	5	30	10	6	25	132.634	133.108	0.474
10	5	30	30	2	25	130.441	133.754	3.313
11	5	10	30	6	35	44.388	43.845	0.543
12	25	10	10	6	35	48.379	48.833	0.454
13	25	30	30	6	35	142.568	141.699	0.869
14	25	30	10	2	35	141.910	141.187	0.723
15	5	10	10	2	25	44.388	44.110	0.278
16	5	30	10	6	35	130.441	130.853	0.412
17	35	20	20	4	30	95.243	93.853	1.390
18	5	30	30	6	35	130.441	131.781	1.340
19	5	30	30	6	25	132.634	133.854	1.220
20	25	10	30	2	25	48.379	50.190	1.811
21	25	30	10	6	35	142.568	141.418	1.150
22	15	20	20	10	30	93.620	92.955	0.665
23	25	10	30	6	25	48.379	49.095	0.716
24	25	10	30	6	35	48.379	48.697	0.318
25	45	20	20	4	30	94.585	96.674	2.089
26	25	20	10	4	40	95.243	94.028	1.557
27	5	10	10	6	25	44.651	43.242	1.409
28	5	10	30	6	25	43.028	41.792	1.236
29	25	30	30	2	35	142.568	141.741	0.827
30	5	30	10	2	25	131.213	133.267	2.054
31	25	30	30	2	25	141.910	142.031	0.121
32	5	10	10	2	35	44.388	44.869	0.481
33	5	30	30	2	35	132.013	131.321	0.692
34	25	30	10	6	25	142.568	141.679	0.889
35	5	10	30	2	25	43.537	42.995	0.542
36	25	10	10	6	25	48.379	48.379	0.000
37	15	20	50	4	30	93.620	93.620	0.000
38	15	20	20	4	30	93.620	93.620	0.000
39	25	50	10	4	40	233.577	233.576	0.001
40	5	10	10	6	35	44.218	44.542	0.324

(*Continued.*)

Table 4. (Continued.)

runs	contact time (min)	initial concentration (mg l^{-1})	adsorbent dosage (mg)	pH	temperature (°C)	experimental, q_e (mg g^{-1})	predicted, q_e (mg g^{-1})	error
41	15	10	10	2	25	46.537	46.537	0.000
42	25	30	30	6	25	142.568	142.180	0.388
43	25	30	10	2	25	142.568	142.568	0.000
44	25	20	10	4	35	48.379	48.379	0.000

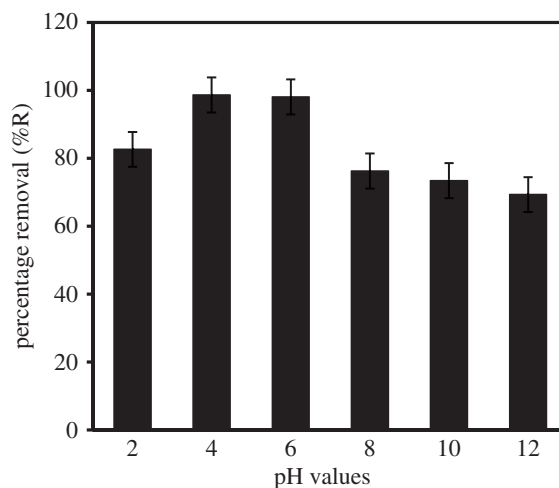**Figure 4.** Effect of solution pH for MCPA removal (dosage: 20 mg; concentration, 20 mg l^{-1}; temperature, 40°C; equilibrium time, 25 min; r.p.m.: 150).
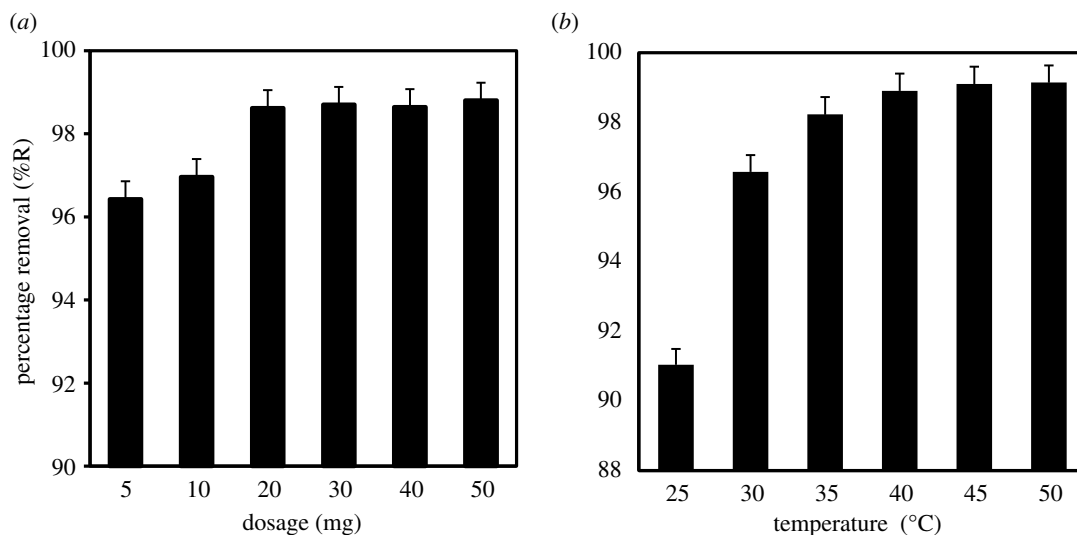

Figure 5. (a) Effect of adsorbent dose and (b) temperature on MCPA removal (concentration, 20 mg l^{-1}; pH, 4; equilibrium time, 20 min; r.p.m.: 150).

low pH (4–6) because of the attraction of the negatively charged pollutant in the solution with a positive surface of the MOF adsorbent. Therefore, the mechanism of MCPA adsorption onto MIL-101(Cr) can be attributed to the electrostatic interaction. At neutral and alkaline pH (7–12), the surface of MIL-101(Cr) is negatively charged, leading to electrostatic repulsion with a gradual decrease in the adsorption capacity.

Table 5. Thermodynamic parameters for the adsorption of dicamba onto MIL-101(Cr).

temp (°C)	$\Delta G°$ (kJ mol^{-1})	$\Delta H°$ (kJ mol^{-1})	$\Delta S°$ (kJ mol^{-1} K^{-1})
25	−127.856	28.334	428.952
30	−130.007		
35	−132.145		
40	−134.290		
45	−136.753		
50	−138.902		

Table 6. Isotherm parameters for adsorption onto MIL-101(Cr).

isotherm model	parameters	MIL-101(Cr) MCPA
Langmuir	q_m (mg g^{-1})	370.37
	K_L (l mg^{-1})	0.45
	R_L	0.1
	R^2	0.92
	R^2 adj	0.899
	RMSE	0.001
	AIC	−80.57
Freundlich	K_F (mg g^{-1})	7.524
	n	1.444
	R^2	0.999
	R^2 adj	0.997
	RMSE	0.023
	AIC	−48.017
Temkin	A (mg g^{-1})	8.253
	bT (kJ mol^{-1})	62.105
	R^2	0.914
	R^2 adj	0.893
	RMSE	26.597
	AIC	40.937

3.3.2. Effect of adsorbent dosage

The amount of adsorbent dose that is sufficient for the removal of pollutants in water can be determined by varying the loading. In this study, the dose of MIL-101(Cr) was varied from 5 to 50 mg in 50 ml solution containing 20 mg l^{-1} of MCPA at 40°C. High recovery efficiency (96.4%) was obtained even at the smallest dosage of 5 mg. As the adsorbent dose increases from 10 to 50 mg, the removal efficiency also increased to 98.8% due to the availability of vacant and active adsorption sites. Figure 5a shows that 20 mg is the optimum dose for the removal of MCPA in water. Thus, 20 mg of MIL-101(Cr) adsorbent was adopted for all the subsequent experiments.

3.3.3. Effect of temperature and thermodynamics

The temperature at which adsorption takes place plays an important role in the removal process. Thus, the effect of temperature (25–50°C) on the adsorption efficiency was investigated and the results are displayed in figure 5b. The positive correlation between temperature and adsorption efficiency implies that the removal of MCPA increases with an increase in temperature. This is because the increase in
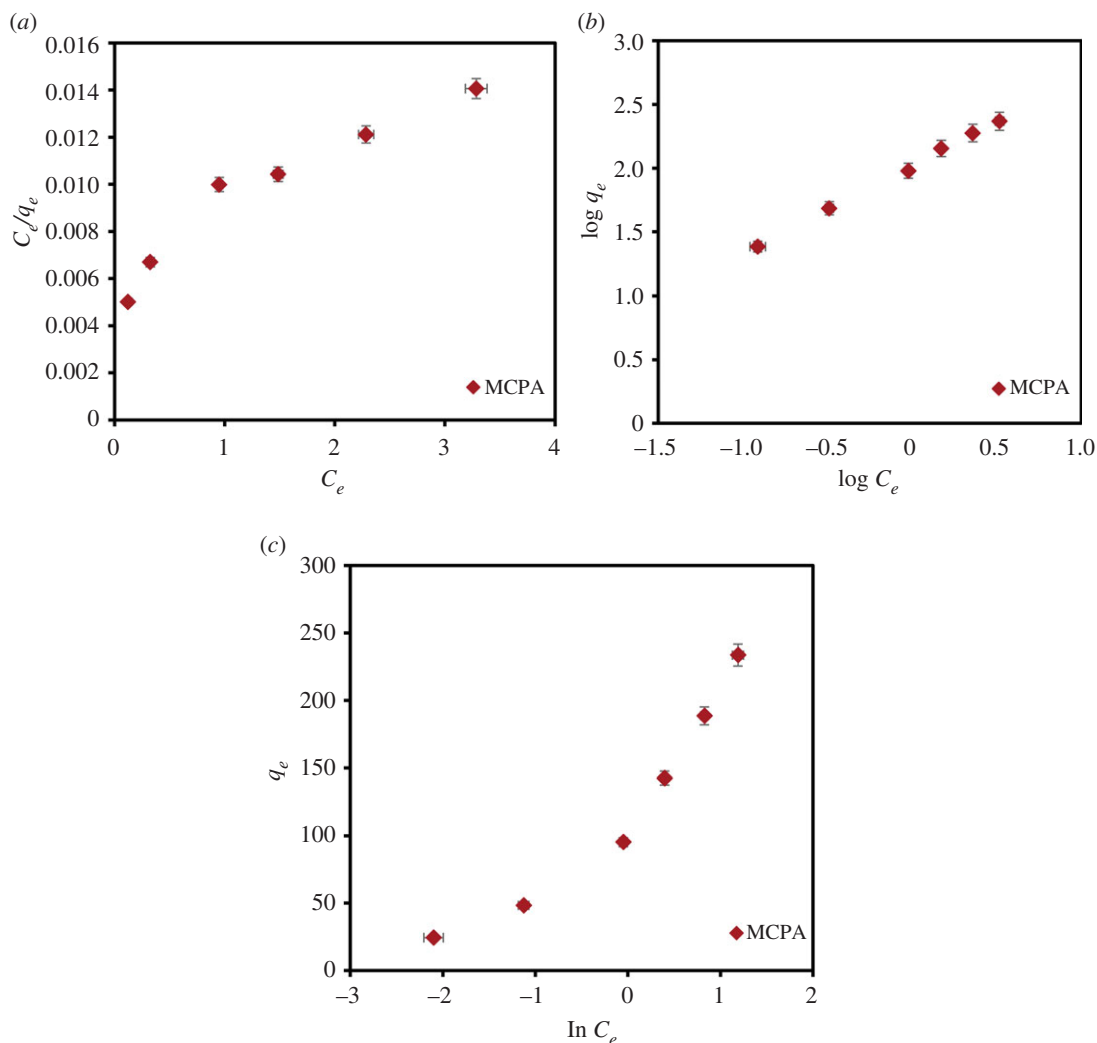
Figure 6. (a) Langmuir, (b) Freundlich and (c) Temkin isotherm for the removal of MCPA (dosage: 20 mg; concentration, 20 mg l^{-1}; temperature, 40°C; equilibrium time, 20 min; r.p.m.: 150).

the temperature will reduce the viscosity of the solution, which allows easy mobility of the adsorbate molecules [46]. Also, the rise in temperature improves the surface activities and pore capacity of the adsorbent as well as the kinetic energy of the solution. Table 5 shows the thermodynamic parameters. The negative values of the Gibbs free energy ($\Delta G°$) represent a spontaneous adsorption process. The adsorption is endothermic due to the positive enthalpy value.

3.3.4. Adsorption isotherm

In this study, the equilibrium data for the removal of MCPA by MIL-101(Cr) were fitted using the Langmuir, Freundlich and Temkin isotherms. The data obtained from the fitted models are presented in table 6 and figure 6a–c). From the results calculated, the Freundlich isotherm model best fit the adsorption process based on the regression analysis with the highest R^2 (0.999), R^2adj (0.997); lowest RMSE (0.023); and the least AIC (−48.017) values. The Freundlich model implies an adsorption process on heterogeneous surfaces with binding sites that are not equivalent.

3.3.5. Effect of contact time and adsorption kinetics

The impact of contact time in the removal of MCPA by MIL-101(Cr) using different concentrations (5–50 mg l^{-1}), contact time (5–60 min), pH (pH 4), adsorbent dose and temperature conditions (pH 3, 20 mg and 40°C) is displayed in figure 7. The results obtained show an excellent and rapid removal of the herbicides within short time (5–10 min) due to the good interaction and porous nature of the MOF
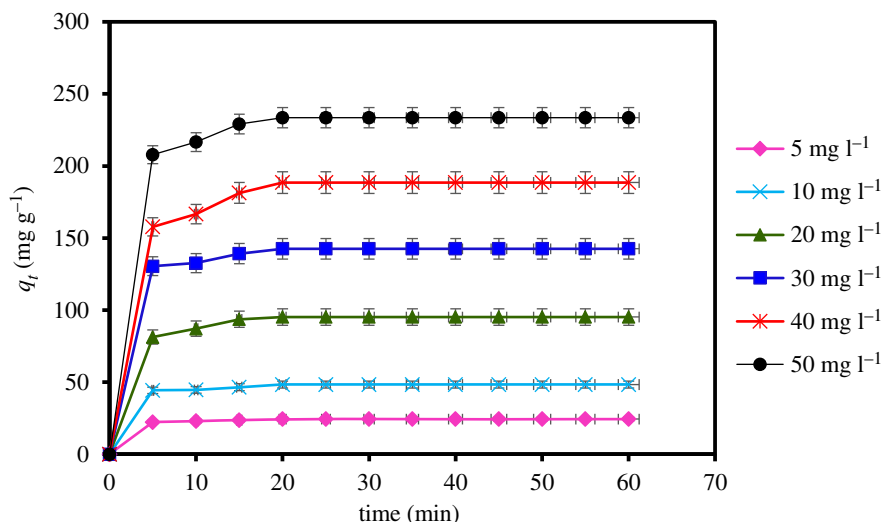
Figure 7. Effect of contact time on MCPA removal (dosage: 20 mg; concentration, 5–50 mg l^{-1}; temperature, 40°C; equilibrium time, 5–60 min; r.p.m.: 150).

adsorbent. This is corroborated by the high BET surface area of the adsorbent (1439 m^2 g^{-1}). Hence, equilibrium was attained within 25 min. The contact time was extended until 60 min to ensure the better interactions of the MOF with the analyte after the equilibrium was established.

To better understand the mechanism of adsorption such as a chemical reaction and mass transfer, the kinetics data were fitted using the pseudo-first-order, pseudo-second-order and intraparticle diffusion models. The kinetics results for the models are displayed in table 7 and figure 8a, which indicate that the pseudo-second-order best fit experimental data have the highest coefficient of determination (R^2 = 0.998), R^2adj = 0.996, lowest RMSE (0.005) and least AIC (–108.511). This is because the q_e values calculated for the pseudo-second-order kinetic are in agreement with the experimental results. The maximum q_e value for MCPA was determined as 233.576 mg g^{-1} at the equilibrium point, which represents the adsorption capacity of MIL-101(Cr). Thus, the result further explains that the adsorption process is controlled by chemical interaction. The intraparticle diffusion mechanism was also used to describe the interaction and the movement of the molecules inside the particles of the MOF adsorbent. Figure 8b indicates two major stages that represent an external diffusion of the pollutant to the surface of the adsorbent and the transport of the molecules from the surface inside the pore of the MOF. This process describes the rate-limiting step of the adsorption.

3.3.6. Reusability studies

The feasibility of MIL-101(Cr) towards the repeated removal of MCPA was studied in view of its regeneration possibility (figure 9). The MOF maintained a steady and high removal efficiency after the third cycle (approx. 98.6%) which indicates better removal capability when compared with the other materials in table 8. A slight decline in the percentage removal (3, 5, 9%) is noticed in the fourth, fifth and sixth cycles, respectively. Nevertheless, the MOF retains approximately 90% removal efficiency after the sixth cycle.

3.3.7. Comparison of different adsorbents for the removal of 4-chloro-2-methylphenoxyacetic acid

Different adsorbents that have been applied for the removal of MCPA in water are summarized in table 8. The superiority of the MIL-101(Cr) adsorbent is readily seen, especially in terms of high surface area, adsorption capacity, % removal efficiency (98.6%), fast equilibration time (approx. 25 min) and prospects for regeneration (approx. 90%) after the sixth cycle.

3.3.8. Possible adsorption mechanisms

Electrostatic interaction is an important mechanism that determines the adsorptive removal of contaminants in water. The positively charged surface of the MOF can easily interact with the negatively charged adsorbate molecules. The solution pH determines the net surface charge of the adsorbent. The high adsorption capacity of MCPA onto MIL-101(Cr) at low pH is attributed to the

Table 7. Adsorption kinetics parameters for the removal of MCPA.

pseudo-first order	mg l⁻¹	$q_{e,exp}$ (mg g⁻¹)	$q_{e,cal}$ (mg g⁻¹)	K_1 (min)⁻¹	R^2	R^2adj	RMSE	AIC
	5	24.388	9.653	0.150	0.783	0.711	0.795	−0.851
	10	48.379	23.203	0.170	0.735	0.647	0.802	−0.767
	20	95.243	66.980	0.225	0.919	0.892	0.558	−4.396
	30	142.568	84.208	0.224	0.821	0.761	0.749	−1.499
	40	188.576	169.236	0.238	0.883	0.844	0.529	−4.917
	50	233.576	170.187	0.253	0.833	0.824	0.644	−2.959

pseudo-second-order MCPA		$q_{e,exp}$ (mg g⁻¹)	q_e cal (g mg⁻¹)	K_2 (g mg⁻¹ min⁻¹)	R^2	R^2adj	RMSE	AIC
	5	24.388	24.390	0.135	0.996	0.995	0.053	−71.372
	10	48.379	48.309	0.059	0.995	0.994	0.026	−81.626
	20	95.243	96.153	0.019	0.998	0.996	0.005	−108.511
	30	142.568	142.857	0.020	0.996	0.995	0.009	−119.225
	40	188.576	188.679	0.010	0.994	0.993	0.007	−126.536
	50	233.576	232.558	0.010	0994	0.993	0.006	−131.463

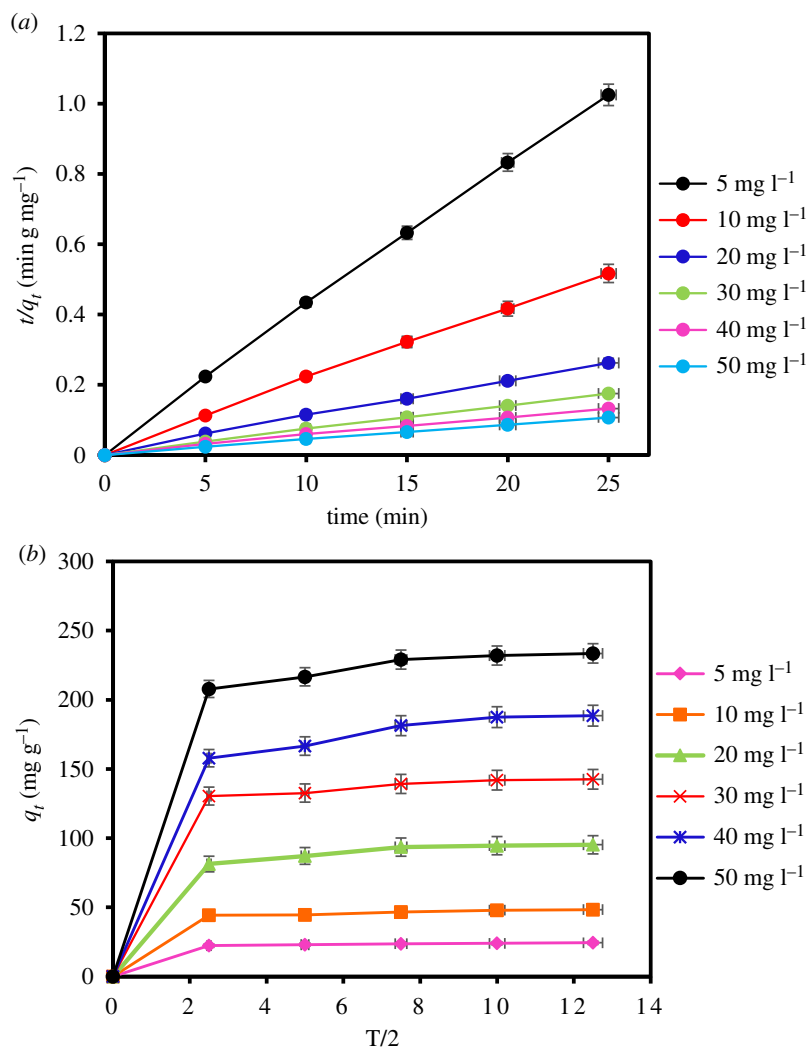| intrapartide diffusion MCPA		K_p (mg⁻¹ g⁻¹ min$^{1/2}$)	C		R^2	R^2adj	RMSE	AIC
	5	2.006	8.658		0.573	0.431	7.904	22.120
	10	3.956	17.01		0.575	0.433	15.536	28.877
	20	8.110	30.922		0.632	0.509	28.263	34.861
	30	11.756	50.189		0.578	0.438	45.828	39.695
	40	16.026	58.755		0.650	0.533	53.666	41.274
	50	19.538	79.755		0.600	0.466	72.833	44.328

Figure 8. (*a*) Pseudo-second-order kinetics and (*b*) intraparticle diffusion model kinetics for MCPA removal (dosage: 20 mg; 40°C; equilibrium time: 25 min; r.p.m.: 150).
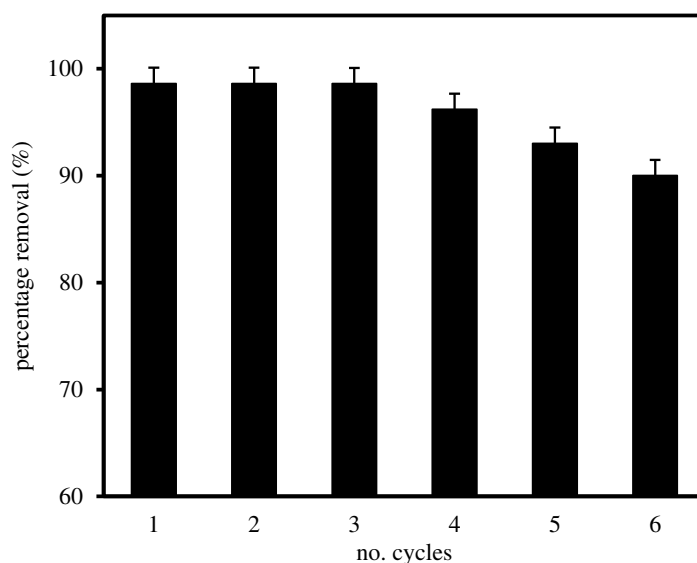

Figure 9. Regeneration and reusability potential of MIL-101(Cr) adsorbent.

Table 8. Adsorbents reported for the removal of MCPA from water.

adsorbent	surface area, ($m^2 g^{-1}$)	concentrations ($mg\,l^{-1}$)	(%) R	Q_e ($mg\,g^{-1}$)	equilibrium time (min)	reuse	ref.
activated carbon	592	50	70	417	210	—	[47]
bentonite	20	1	80–95		1440	—	[48]
biochar	1.1	100	90	28	360	—	[49]
metal hydroxide	nil	50	84	42	240	nil	[50]
NH$_2$@COF	335.7		97.3	11			[51]
vinylCOF	345.4		94.3	2			
MIL-101(Cr)	1439	50	98.62	234	20	5	this work

electrostatic attraction between the MCPA anions and the positively charged surface of the MOF. As the pH increases, the surface charge gradually decreases causing electrostatic repulsion, thus retarding the adsorption process. The fast and feasible adsorption is also attributed to the chemisorption process which is in agreement with the pseudo-second-order kinetics model. The better fitting with the Freundlich isotherm describes a heterogeneous adsorption surface and an exponential distribution of active sites and energies for better adsorption of MCPA onto the MOF.

4. Conclusion

An in-depth assessment of the removal of MCPA using the adsorbent MIL-101(Cr) was conducted by batch experiments. The experimental q_e values for each range of experimental conditions were also predicted by the ANN model with significant correlations and minimal errors. Fast adsorption equilibrium was reached within approximately 25 min using a small dose of the adsorbent material (20 mg). The adsorption process follows the pseudo-second-order kinetics model ($R^2 > 0.998$, RMSE 0.005). The maximum q_e value of the model is 233.576 mg g^{-1}. The intraparticle diffusion model indicated a fast phase, signifying an external diffusion of the MCPA molecules from the solution to the surface of the MOF as the rate-determining step, and the slower phase was followed signifying the adsorption of the MCPA molecules to the internal pores of the MOF, until equilibrium is attained. The adsorption process best fit the Freundlich isotherm (R^2, 0.999; RMSE, 0.023 and AIC, –48.017). In comparison with other previously reported adsorbent materials, MIL-101(Cr) performed well in the removal of MCPA in terms of fast equilibration, removal efficiency, high adsorption capacity and reusability. It is worth noting that the adsorption process and dataset used for the ANN prediction were based on controlled laboratory conditions.

References

1. Starling MCVM, Amorim CC, Leão MMD. 2019 Occurrence, control and fate of contaminants of emerging concern in environmental compartments in Brazil. *J. Hazard. Mater.* **372**, 17–36. (doi:10.1016/j.jhazmat.2018.04.043)

2. Sophia AC, Lima EC. 2018 Removal of emerging contaminants from the environment by adsorption. *Ecotoxicol. Environ. Saf.* **150**, 1–17. (doi:10.1016/j.ecoenv.2017.12.026)

3. Le TDH, Scharmüller A, Kattwinkel M, Kühne R, Schüürmann G, Schäfer RB. 2017 Contribution of waste water treatment plants to pesticide toxicity in agriculture catchments. *Ecotoxicol. Environ. Saf.* **145**, 135–141. (doi:10.1016/j.ecoenv.2017.07.027)

4. Kelly J, Morrison G, Skillen N, Manesiotis P, Robertson PKJ. 2019 An investigation of the role

of pH in the rapid photocatalytic degradation of MCPA and its primary intermediate by low-power UV LED irradiation. *Chem. Eng. J.* **359**, 112–118. (doi:10.1016/j.cej.2018.11.142)

5. Turek M, Pawłowska B, Różycka-Sokołowska E, Biczak R, Skalik J, Owsianik K, Marciniak B, Bałczewski P. 2020 Ecotoxicity of ammonium chlorophenoxyacetate derivatives towards aquatic organisms: unexpected enhanced toxicity upon oxygen by sulfur replacement. *J. Hazard. Mater.* **382**, 121086. (doi:10.1016/j.jhazmat.2019.121086)

6. Muter O, Berzins A, Strikauska S, Pugajeva I, Bartkevics V, Dobele G, Truu J, Truu M, Steiner C. 2014 The effects of woodchip- and straw-derived biochars on the persistence of the herbicide 4-chloro-2-methylphenoxyacetic acid (MCPA) in soils. *Ecotoxicol. Environ. Saf.* **109**, 93–100. (doi:10.1016/j.ecoenv.2014.08.012)

7. López-piñeiro A, Peña D, Albarrán A, Sánchez-llerena J, Becerra D. 2013 Behavior of MCPA in four intensive cropping soils amended with fresh, composted, and aged olive mill waste. *J. Contam. Hydrol.* **152**, 137–146. (doi:10.1016/j.jconhyd.2013.07.003)

8. Wu D, Yun Y, Jiang L, Wu C. 2018 Influence of dissolved organic matter on sorption and desorption of MCPA in ferralsol. *Sci. Total Environ.* **616–617**, 1449–1456. (doi:10.1016/j.scitotenv.2017.10.169)

9. Awad AM, Shaikh SMR, Jalab R, Gulied MH, Nasser MS, Benamor A, Adham S. 2019 Adsorption of organic pollutants by natural and modified clays: a comprehensive review. *Sep. Purif. Technol.* **228**, 115719. (doi:10.1016/j.seppur.2019.115719)

10. Wei C, Feng D, Xia Y. 2016 Fast adsorption and removal of 2-methyl-4-chlorophenoxy acetic acid from aqueous solution with amine functionalized zirconium metal-organic framework. *RSC Adv.* **6**, 96 339–96 346. (doi:10.1039/c6ra18520g)

11. Solís RR, Rivas FJ, Martínez-Piernas A, Agüera A. 2016 Ozonation, photocatalysis and photocatalytic ozonation of diuron: intermediates identification. *Chem. Eng. J.* **292**, 72–81. (doi:10.1016/j.cej.2016.02.005)

12. World Health Organization. 2015 *Water sanitation hygiene, water supply and sanitation monitoring and evidence, key facts from JMP 2015 report*. See https://www.who.int/water_sanitation_health/monitoring/jmp-2015-key-facts/en/.

13. Spaltro A, Pila M, Simonetti S, Álvarez-Torrellas S, Rodríguez JG, Ruiz D, Compañy AD, Juan A, Allegretti P. 2018 Adsorption and removal of phenoxy acetic herbicides from water by using commercial activated carbons: experimental and computational studies. *J. Contam. Hydrol.* **218**, 84–93. (doi:10.1016/j.jconhyd.2018.10.003)

14. Sun Y, Cao M, Wan Y, Wang H, Liu J, Pan F, He W, Huang H, He Z. 2020 Spatial variation of 2,4-D and MCPA in tap water and groundwater from China and their fate in source, treated, and tap water from Wuhan, Central China. *Sci. Total Environ.* **727**, 138691. (doi:10.1016/j.scitotenv.2020.138691)

15. Mantasha I, Saleh HAM, Qasem KMA, Shahid M, Mehtab M, Ahmad M. 2020 Efficient and selective adsorption and separation of methylene blue (MB) from mixture of dyes in aqueous environment employing a Cu(II) based metal organic framework. *Inorganica Chim. Acta* **511**, 119787. (doi:10.1016/j.ica.2020.119787)

16. Anastopoulos I, Pashalidis I, Orfanos AG, Manariotis ID, Tatarchuk T, Sellaoui L, Bonilla-Petriciolet A, Mittal A, Núñez-Delgado A. 2020 Removal of caffeine, nicotine and amoxicillin from (waste)waters by various adsorbents. A review. *J. Environ. Manage.* **261**, 131–139. (doi:10.1016/j.jenvman.2020.110236)

17. Derylo-marczewska A, Blachnio M, Marczewski AW, Swiatkowski A. 2017 Adsorption of chlorophenoxy pesticides on activated carbon with gradually removed external particle layers. *Chem. Eng. J.* **308**, 408–418. (doi:10.1016/j.cej.2016.09.082)

18. Loklindt N, Nikbakht M, Krisztian P, Mu J. 2019 Synergy of combined adsorption and electrochemical degradation of aqueous organics by granular activated carbon particulate electrodes. *Sep. Purif. Technol.* **208**, 51–58. (doi:10.1016/j.seppur.2018.05.023)

19. Cederlund H, Börjesson E, Lundberg D, Stenström J. 2016 Adsorption of pesticides with different chemical properties to a wood biochar treated with heat and iron. *Water Air Soil Pollut.* **203**, 1–12. (doi:10.1007/s11270-016-2894-z)

20. Iglesias A, López R, Gondar D, Antelo J, Fiol S, Arce F. 2010 Adsorption of MCPA on goethite and humic acid-coated goethite. *J. Hazard. Mater.* **183**, 664–668. (doi:10.1016/j.jhazmat.2010.07.077)

21. Gusain R, Kumar N, Ray SS. 2020 Recent advances in carbon nanomaterial-based adsorbents for water purification. *Coord. Chem. Rev.* **405**, 213111. (doi:10.1016/j.ccr.2019.213111)

22. Liu X, Valentine HL, Pan W, Cao Y, Yan B. 2016 2D metal–organic frameworks: syntheses, structures, and electrochemical properties. *Inorganica Chim. Acta* **447**, 162–167. (doi:10.1016/j.ica.2016.03.048)

23. Batten SR, Champness NR. 2017 Coordination polymers and metal-organic frameworks: materials by design. *Phil. Trans. R. Soc. A* **375**, 20160032. (doi:10.1098/rsta.2016.0032)

24. Dhaka S, Kumar R, Deep A, Kurade MB, Ji SW, Jeon BH. 2019 Metal–organic frameworks (MOFs) for the removal of emerging contaminants from aquatic environments. *Coord. Chem. Rev.* **380**, 330–352. (doi:10.1016/j.ccr.2018.10.003)

25. Dunne LJ, Manos G. 2018 Statistical mechanics of binary mixture adsorption in metal-organic frameworks in the osmotic ensemble. *Phil. Trans. R. Soc. A* **376**, 20170151. (doi:10.1098/rsta.2017.0151)

26. Samokhvalov A. 2018 Aluminum metal–organic frameworks for sorption in solution: a review. *Coord. Chem. Rev.* **374**, 236–253. (doi:10.1016/j.ccr.2018.06.011)

27. Opeyemi K. 2020 Temperature-controlled activation and characterization of iron-based metal-organic frameworks. *Inorganica Chim. Acta* **507**, 119563. (doi:10.1016/j.ica.2020.119563)

28. Maksimchuk NV, Zalomaeva OV, Skobelev IY, Kovalenko KA, Fedin VP, Kholdeeva OA. 2012 Metal-organic frameworks of the MIL-101 family as heterogeneous single-site catalysts. *Proc. R. Soc. A* **468**, 2017–2034. (doi:10.1098/rspa.2012.0072)

29. Kang IJ, Khan NA, Haque E, Hwa S. 2011 Chemical and thermal stability of isotypic metal–organic frameworks: effect of metal ions. *Eur. J.* **4**, 6437–6442. (doi:10.1002/chem.201100316)

30. Mirsoleimani-Azizi SM, Setoodeh P, Samimi F, Shadmehr J, Hamedi N, Rahimpour MR. 2018 Diazinon removal from aqueous media by mesoporous MIL-101(Cr) in a continuous fixed-bed system. *J. Environ. Chem. Eng.* **6**, 4653–4664. (doi:10.1016/j.jece.2018.06.067)

31. Karmakar S, Roy D, Janiak C, De S. 2019 Insights into multi-component adsorption of reactive dyes on MIL-101-Cr metal organic framework: experimental and modeling approach. *Sep. Purif. Technol.* **215**, 259–275. (doi:10.1016/j.seppur.2019.01.013)

32. Gao Y, Liu K, Kang R, Xia J, Yu G, Deng S. 2018 A comparative study of rigid and flexible MOFs for the adsorption of pharmaceuticals: kinetics, isotherms and mechanisms. *J. Hazard. Mater.* **359**, 248–257. (doi:10.1016/j.jhazmat.2018.07.054)

33. Gadekar MR, Ahammed MM. 2019 Modelling dye removal by adsorption onto water treatment residuals using combined response surface methodology-artificial neural network approach. *J. Environ. Manage.* **231**, 241–248. (doi:10.1016/j.jenvman.2018.10.017)

34. G. Férey, C. Mellot-Draznieks, C. Serre, F. Millange, J. Dutour SS, I. Margiolaki. 2005 A chromium terephthalate-based solid with unusually large pore volumes and surface area. *Science* **309**, 2040–2042. (doi:10.1126/science.1117808)

35. Altowayti WAH, Algaifi HA, Bakar SA, Shahir S. 2019 The adsorptive removal of As (III) using biomass of arsenic resistant *Bacillus thuringiensis* strain WS3: characteristics and modelling studies. *Ecotoxicol. Environ. Saf.* **172**, 176–185. (doi:10.1016/j.ecoenv.2019.01.067)

36. Isiyaka HA, Juahir H, Phil- P. 2019 Water quality modelling using artificial neural network and multivariate statistical techniques. *Model Earth Sys. Environ.* **5**, 583–593. (doi:10.1007/s40808-018-0551-9)

37. Banerjee P, Sau S, Das P, Mukhopadhayay A. 2015 Optimization and modelling of synthetic azo dye wastewater treatment using graphene oxide nanoplatelets: characterization toxicity evaluation and optimization using artificial neural network. *Ecotoxicol. Environ. Saf.* **119**, 47–57. (doi:10.1016/j.ecoenv.2015.04.022)

38. Yusuf M, Song K, Li L. 2020 Fixed bed column and artificial neural network model to predict heavy metals adsorption dynamic on surfactant decorated graphene. *Colloids Surfaces A* **585**, 225–240. (doi:10.1016/j.colsurfa.2019.124076)

39. Zango ZU, Jumbri K, Sambudi NS, Hanif Abu Bakar NH, Fathihah Abdullah NA, Basheer C,

Saad B. 2019 Removal of anthracene in water by MIL-88(Fe), NH$_2$-MIL-88(Fe), and mixed-MIL-88(Fe) metal-organic frameworks. *RSC Adv.* **9**, 41 490–41 501. (doi:10.1039/c9ra08660a)

40. Delgado N, Capparelli A, Navarro A, Marino D. 2019 Pharmaceutical emerging pollutants removal from water using powdered activated carbon: Study of kinetics and adsorption equilibrium. *J. Environ. Manage.* **236**, 301–308. (doi:10.1016/j.jenvman.2019.01.116)

41. Jafar S, Sedigheh Z, Maryam T. 2019 Synthesis of a chromium terephthalate metal organic framework and use as nanoporous adsorbent for removal of diazinon organophosphorus insecticide from aqueous media. *J. Dispers. Sci. Technol.* **40**, 1–18. (doi:10.1080/01932691.2018.1516149)

42. Masood SA, Marzieh Shafiei-Alavijeh NHMHT, Ebrahim G, Alimorad RSF. 2019 Facile and high-yield synthesis of improved MIL-101 (Cr) metal-organic framework with exceptional CO$_2$ and H$_2$S uptake; the impact of excess ligand-cluster. *Microporous Mesoporous Mater.* **279**, 153–164. (doi:10.1016/j.micromeso.2018.12.033)

43. Niknam E, Panahi F, Daneshgar F, Bahrami F. 2018 Metal–organic framework MIL-101(Cr) as

an efficient heterogeneous catalyst for clean synthesis of benzoazoles. *ACS Omega* **3**, 17 135–17 144. (doi:10.1021/acsomega.8b02309)

44. Liu Q, Ning L, Zheng S, Tao M, Shi Y, He Y. 2013 Adsorption of carbon dioxide by MIL-101 (Cr): regeneration conditions. *Sci. Rep.* **2**, 1–6. (doi:10.1038/srep02916)

45. Uddin Z, Yao L, Lian Q, Islam F, Zappi ME, Dianchen D. 2020 The use of artificial neural network (ANN) for modeling adsorption of sunset yellow onto neodymium modified ordered mesoporous carbon. *Chemosphere* **256**, 127081. (doi:10.1016/j.chemosphere.2020.127081)

46. Shahnaz T, Sharma V, Subbiah S, Narayanasamy S. 2020 Multivariate optimisation of Cr (VI), Co (III) and Cu (II) adsorption onto nanobentonite incorporated nanocellulose/chitosan aerogel using response surface methodology. *J. Water Process Eng.* **36**, 101283. (doi:10.1016/j.jwpe.2020.101283)

47. Pandiarajan A, Kamaraj R, Vasudevan S. 2018 OPAC (orange peel activated carbon) derived from waste orange peel for the adsorption of chlorophenoxyacetic acid herbicides from water: adsorption isotherm, kinetic modelling and

thermodynamic studies. *Bioresour. Technol.* **261**, 329–341. (doi:10.1016/j.biortech.2018.04.005)

48. Durán E, Bueno S, Hermosín MC, Cox L, Gámiz B. 2019 Optimizing a low added value bentonite as adsorbent material to remove pesticides from water. *Sci. Total Environ.* **672**, 743–751. (doi:10.1016/j.scitotenv.2019.04.014)

49. Essandoh M, Wolgemuth D, Pittman CU, Mohan D, Mlsna T. 2017 Phenoxy herbicide removal from aqueous solutions using fast pyrolysis switchgrass biochar. *Chemosphere* **174**, 49–57. (doi:10.1016/j.chemosphere.2017.01.105)

50. Kamaraj R, Davidson DJ, Sozhan G, Vasudevan S. 2014 An in situ electrosynthesis of metal hydroxides and their application for adsorption of 4-chloro-2-methylphenoxyacetic acid (MCPA) from aqueous solution. *J. Environ. Chem. Eng.* **2**, 2068–2077. (doi:10.1016/j.jece.2014.08.027)

51. Ji WH, Guo YS, Wang X, Lu XF, Guo DS. 2019 Amino-modified covalent organic framework as solid phase extraction absorbent for determination of carboxylic acid pesticides in environmental water samples. *J. Chromatogr. A* **1595**, 11–18. (doi:10.1016/j.chroma.2019.02.048)